L C Lund-Hansen, T Juul, T D Eskildsen, I Hawes, B Sorrell, C Melvad, K Hancke. A low-cost remotely operated vehicle (ROV) with an optical positioning system for under-ice measurements and sampling. Volume 151, 2018, pages 148-155, ISSN 0045-6535.

The article has been published in final form by Elsevier at http://dx.doi.org/10.1016/j.coldregions.2018.03.017

A low-cost remotely operated vehicle (ROV) with an optical positioning system for investigating under-ice irradiance fields in landfast sea ice

Lars Chresten Lund-Hansen*[1,2], Thomas Juul[3], Tor Dam Eskildsen[3], Ian Hawes[4], Brian Sorrell[1,2], Claus Melvad[3], Kasper Hancke[1,5]

[1]Aquatic Biology, Department of Bioscience, Aarhus University, Build. 1134, Ole Worms Allé 1, 8000 Aarhus C, Denmark

[2]Arctic Research Centre, Department of Bioscience, Aarhus University, Build. 1540, Ny Munkegade 114, 8000 Aarhus C, Denmark

[3]School of Engineering, Aarhus University, Inge Lehmanns Gade 10, 8000 Aarhus C, Denmark

[4]Coastal Marine Field Station, University of Waikato, Sulphur Point Tauranga 3110, New Zealand

[5]Norwegian Institute for Water Research (NIVA), Research Centre for Coast and Ocean, Gaustadalléen 21, N-0349 Oslo, Norway

*Corresponding author: lund-hansen@bios.au.dk

ABSTRACT

Here we describe the design, performance and field tests of a lightweight (13.1 kg), low-cost (15.000 USD), and portable remotely operated vehicle (ROV) of dimensions 55×43×34 cm (L×H×W), with a new optical based positioning system. The ROV is designed for deployments and measurements of the irradiance field at a short distance below sea ice bottom in landfast level sea ice at calm under ice conditions. It is equipped with two cameras (front and rear) for optical positioning based on reference poles with LED lights below the ice. A third upward camera is for guiding during deployment and positioning. The ROV is equipped with spacer poles to maintain a constant distance between ROV with onboard optical sensors and bottom of the ice. All pre-tests of housing, thrusters, optical positioning, and ROV maneuverability were carried out in freshwater basins prior to field trials and tests. These were conducted at Kangerlussuaq, West Greenland on landfast first-year 79-80 cm thick ice with a variable (1-12 cm) snow cover in March 2016. The ROV was easily deployed through a hole (75 × 50 cm) in the ice and easy to maneuver below the ice. Test of positioning system showed an average deviation of 28 ± 5 cm between optically based position and actual position with an average offset from center line of 16 ± 5 cm. The ROV was applied for measuring the under-ice irradiance field and results demonstrated a solid negative correlation between snow depth and PAR transmittance. We derived a Normalized Differences Index (NDI) for snow depths: $NDI_{snow\ depth} = [E(610\ nm) – E(490\ nm)]/[E(610\ nm) + E(490\ nm)]$ with minimum attenuation at 490 nm and maximum at 610 nm. It is discussed that the correlations for both PAR transmittance and the NDI with snow depths are due to a combination of a constant distance between optical sensor and ice bottom, and accurate positioning. A test showed that the wakes of thrusters removed parts of the ice algae biomass, but the study demonstrates the applicability of this ROV design for measurements of the under-ice irradiance field below landfast sea ice with a new optical based positioning system.

Keywords: ROV; Sea ice; Snow; Transmittance; NDI; Greenland

1. Introduction

A variety of Remotely Operated Vehicles (ROVs) have been used in the polar regions for research either using ship based platforms, or operated directly from the ice through a hole, or in leads in the ice. ROVs are particularly well-suited for under-ice missions in that they allow access to an area/environment otherwise difficult to access, and minimize disturbance of the ice environment compared to traditional coring methods. ROVs further enable operations across a range of temporal and spatial resolutions, and perform measurements of key under-ice variables that would be difficult to obtain by any other methods (Moore et al., 1986; Christ and Wernli, 2013). ROV-based research in polar regions has been applied for assessing the spatial variability of sea ice thickness (Wadhams, 2012), for physical, chemical and biological water sampling close to icebergs (Hobson et al., 2011), study their micro algae communities (Robison et al., 2011), and Antarctic benthic communities (Cazenave et al., 2011). At the ice-water interface ROVs have been deployed for imaging of ice algae (Ambrose et al., 2005), ice algae aggregates (Katlein et al., 2015), for mapping under-ice irradiance, transmittance, and ice algae distributions (*e.g.* Mundy et al., 2007; Nicolaus and Katlein, 2013; Bowen et al., 2014; Katlein et al., 2015b; Lange et al., 2016; Taskjelle et al., 2016; Arndt et al., 2017; Katlein et al., 2017; Meiners et al. 2017). An advantage of ROVs over traditional techniques of through-hole sampling is their ability to obtain measurements and images across large spatial scales and non-invasively, in contrast to the traditional invasive drilling of ice cores with limited spatial resolution. Transmittance through the ice and irradiances at the bottom of the ice are the main parameters explaining the spatial distribution of ice algae, with their photosynthesis being limited by irradiance and less by nutrients (Arrigo and Sullivan, 1994; Mundy et al., 2005; Arrigo et al., 2010). Under-ice irradiance is regulated by the optical properties of the ice and snow (*e.g.* Perovich et al., 1998; Nicolaus and Katlein, 2013, Lund-Hansen et al., 2013; Katlein et al., 2015b; Taskjelle et al., 2016) and studies have established negative relations between snow depth and ice algae biomass (Juhl and Krembs, 2010; Mundy et al., 2005). There is, in this respect, a need for more detailed and accurate measurements and descriptions of under-ice PAR and spectral transmittance distributions that can be applied in the Arctic primary production models. Achieving this also requires replacement of the standard core-based point-sampling method of PAR and spectral transmittance based on through-hole and L-arm techniques (Lund-Hansen et al., 2013, Lange et al., 2016). For ROV-based remote sensing of snow and sea ice transmittance, it is specifically required that under-ice PAR and spectral irradiance can be obtained at accurate positions. ROVs flying depths for under-ice irradiance is typically 1-2 m below the bottom of the ice (Katlein et al., 2015b; Lange et al., 2016). Under-ice transmittance has been mapped with constant distances between sensor head and the ice but with no precise positioning and reduced maneuverability (Nicolaus et al., 2013; Taskjelle et al., 2016). The radiometer sledge developed by Nicolaus et al. (2013) with a constant distance between ice and sensor head of 2 cm had a positioning accuracy of < 1.0 m. We have constructed a novel, lightweight, and very low-cost ROV equipped with a new positioning system that allows decimeter-scale positioning accuracy over underwater transects of at least 15 m. The ROV is easily deployed through a hole in the ice and can place optical instruments at a precise and constant vertical distance to the bottom of the ice at all positions using spacer poles. The ROV was designed and developed for landfast level sea ice and here we describe the ROV, validate its positioning accuracy, and demonstrate its use for obtaining PAR and spectral transmittance under landfast level sea ice at Kangerlussuaq, West Greenland.

2 Materials and procedures

2.1. ROV design

The outer frame of the ROV was a blend of polycarbonate and aluminum parts on which the thrusters and canister were mounted (Figs. 1a-c). Dimensions of the ROV were (55×43×34 cm L×H×W) with an in-air weight of 13.1 kg. The canister was custom-made from milled aluminum and acrylic pipe, and housed the electronics and the three cameras. The main floats (yellow) were made of extruded polystyrene with closed cell structures for buoyancy. Additional floats made of polyethylene foam material (grey) and also with closed cell structures were mounted on site to trim the ROV to keep a weak positive buoyancy (Fig. 1a). At position the ROV drifts towards the bottom of the ice with thrusters turned off in order not to cause any disturbance of the ice algae. Vertical thrusters were turned on when leaving the position to circumvent the weak positive buoyancy. The ROV was powered through the tether by an external power supply (here we used a gasoline driven Honda EC2000 2.0 KW). The ROV was equipped with three cameras: one for recovery (Pointgrey Blackfly, BFLY-PGE-12A2C-CS, 1280×960 pixels) and two for positioning (Pointgrey Blackfly, BFLY-PGE-50A2C-CS (2592×1944), Richmond, BC, Canada, http://www.ptgrey.com). The positioning cameras were mounted with lenses (Fujifilms, Fujinon HF9HA-1B, Tokyo, Japan, http://www.fujifilmusa.com), with one facing forwards and one backwards for positioning and direct visual feedback (Fig. 1a-c). The third camera was facing upwards and equipped with a fish-eye lens (Lensation, Lensagon BF5M13720, Karlsruhe, Germany, http://www.lensation.de) and used to maneuver the ROV during deployments and recovery. Maneuvering was executed with six thrusters (Blue Robotics T200 Thrusters, Torrance, California, U.S., http://www.bluerobotics.com), with four of the thrusters mounted in a vectored configuration. A configuration where the length axis of the thrusters is oriented 45° relative to the center axis of the ROV for optimum control and stability in the horizontal direction. The remaining two were oriented vertically for pitch, roll, and depth control. An auto-depth module, which operates via the onboard pressure transducer (Type 4130A0.2, Kistler, Herfølge, Denmark, http://www.kistler.com), maintained a constant depth at horizontal movements. The vertical thrusters were placed underneath the housing to minimize any influence of the wake of the thrusters during operation and deployments (Fig. 1c). A control room was set up in a tent on the ice where an operator maneuvered the ROV based on live-feed information from the three ROV cameras, depth recordings, and positioning data (Fig. 1d). A group of five persons tested the ROV at several sites and it took about one hour to drill the hole in the ice, set up the control room, and place the LED reference poles at each end of the transect of interest. All control of the ROV was manual, using a X-box Controller (Wired USB gamepad controller for Microsoft Xbox 360, http://www.microsoft.com). Navigation data comprised three live-feed signals from the cameras, depth, and output data from the positioning system. Data were displayed and processed on a laptop PC, in a program developed by the authors using LabVIEW's Real Time Module (LabVIEW, Austin, Texas, USA, http://www.ni.com). The electronics in the housing were kept above freezing point by the generated heat from the internal DC-stepdown voltage converters. A tether facilitated electric power to the ROV, and data transmission (Ethernet) between control room laptop PC and ROV. The tether consisted of three separate cables bundled into one with cable ties around a metal wire. Small floats were mounted at about every 1 m along the tether to keep neutral buoyancy and minimize drag. The ROV was parked at positions under the sea ice with the spacer poles resting against the bottom of the ice, which ensured a constant and small distance between optical sensors and the ice at all positions (Fig. 1c). The weak positive buoyancy of the ROV allowed the spectroradiometric measurements to be carried out with all thrusters turned off and the ROV parked at constant positions below the ice. The maximum ROV working range was initially developed and designed to 30 m but was changed to 15 m during tests due to unexpected high attenuation in the water (Fig. 1d). The ROV was kept in a heated and insulated box between deployments in the control room. This was to prevent freezing of water around thrusters, which might be damaged at the low air temperatures (minus 5-20 °C). The total material cost was about 15.000 USD. Technical details concerning brands, specifications, and calibration of the positioning system can be found as Supplementary Material.

2.2. Positioning system

Reference poles with LED lights were mounted through holes in the ice at either end of an experimental transect for positioning of the ROV (Figs. 1b-d). The poles were constructed of polyoxymethylen (POM) to prevent freezing into the ice as we had to relocate between different test sites and remove poles. Each pole contained two LEDs in aluminum housing for protection, and to ensure a high thermal conductivity of generated heat by the LEDs, in order to avoid any damage of the LEDs. The depth of the poles was adjusted by horizontally mounted aluminum rods at the top of the poles (Fig. 1b). The LEDs were powered via the surface power supply – the Honda generator. The positioning system was designed to allow the ROV to navigate in 2D with respect to the two reference poles, each equipped with two strong lights visible to the front and rear cameras on the ROV (Fig. 1d). The two reference poles were positioned at each end of the ROV transect with the LED lights pointing towards the ROV. The real time positioning system of the ROV was based on image processing of live-feed digital images from front and rear cameras on the ROV with the LEDs positioned at the end and beginning of the transect (Fig. 1d). Centroids of

LED lights were detected through image processing, from which vertical pixel distance between the LEDs (px_v) and the average horizontal offset from the vertical center of the field of view (px_h) was determined (Fig. 2a). The LED pixel distance (px_v) was converted to distance based on a relation established previously during ROV tests in a freshwater basin. This is also the case with the relation between (px_h) and angle (α) between line of reference point and center of field of view (Fig. 2b). The angle (α) was obtained from both the front (α_f) and the rear (α_r) cameras. Calculation of an along transect position was based on the two angles (α_f) and (α_r), and the distance to a reference pole (D_2), which was derived from the image processing, and the known distance (D_1) between reference poles (Fig. 2c). The D_2 is the distance to the nearest LED pole.

2.3. Payload

The ROV was equipped with a spectroradiometer (TriOS RAMSES ACC-UV/VIS, Rastede, Germany, http://www.trios.de) measuring between 320-950 nm with a spectral resolution of 3.3 nm in a titanium housing (Fig. 1a). The sensor was connected to a ruggedized field computer in the control room and data were acquired using the company (TriOS) delivered software MSDA_XE version 8.8.13. Data were transmitted through an independent cable attached to the ROV tether. The spectroradiometer sensor was calibrated immediately prior to the campaign by the company. The GoPro camera (GoPro 4.0 Black Edition, Santa Mateo, California, U.S., http://www.gopro.com) mounted on the canister is applied for video and still images recording of under-ice conditions (Fig. 1a). The blue sensor near the GoPro camera is a self-contained PAR sensor (Dataflow Systems, Christchurch, New Zealand, http://www.odysseydatarecording.com) for continuous PAR recording.

2.4. Field tests

The ROV was tested and deployed below the sea ice in Kangerlussuaq (66° 56.37' N; 50° 59.28' W), West Greenland, in March 2016 under landfast 79-80 cm thick level first-year ice. A detailed description of the Kangerlussuaq test site is given by Nielsen et al. (2010) and Lund-Hansen et al. (2013). To deploy the ROV under the sea ice we cut a hole (75 × 50 cm) in the ice with a motorized Jiffy 25 cm ice drill (http://www.jiffyonice.com) and a manual ice saw (http://www.landmsupply.com), tailored to the dimensions of the ROV. ROV tests and under-ice deployments are demonstrated in a video (http://dx.doi.org/10.17632/rt4nd5bw5c.1). We performed two field positioning tests - A and B.

2.5. Test A

During test A we tested the ability of the ROV to navigate at known and accurate positions. The ROV was placed at a position on a transect based on the read-out from the imaging positioning system with spacer poles resting against the bottom of the ice. To evaluate the performance we carefully drilled a hole with a Kovacs 5 cm driller (http://www.kovacsicedrillingequipment.com) through the ice at the image based position to check whether the drilled hole was visible to the upward-directed camera on the ROV. The footprint of the camera with the fisheye lens was a circle with a radius of about 35 cm in which the spacer poles rectangle (34 × 55 cm) was clearly visible. The criterion for approval was a visible hole as observed from the camera.

2.6. Test B

Test B comprised drilling of eight 5 cm holes along a snow free line between the two reference poles. Distances from the reference pole to each of the holes were measured to nearest 1 cm. A red plastic pole was inserted through the hole and the ROV was maneuvered and parked at a position where the stick would touch the front of the ROV between the front spacer poles using the upward directed camera. The accuracy of the ROV positioning system was quantified as the difference between the tape measured position of the hole, and the position read-out from the ROV positioning system along the transect line. ROV offset, *i.e.* the perpendicular distance between poles line and center axis of the ROV (Fig. 2c), was given as the distance between poles line and optical based position of the ROV.

2.7. Ice algae biomass and flow simulations

A risk with ROVs at short distances to the object of interest is that the wakes of the thrusters may disturb or eventually remove the object (Christ and Wernli, 2013), in this case the ice algae at the bottom of the sea ice, that could potentially be flushed away. We investigated the question by performing a CFD (Computational Fluid Dynamics) simulation followed by field tests. The simulation applying SolidWorks Flow Simulation software (http://www.solidworks.com) was based on a scenario with a simplified model of the ROV at a constant distance of 25 cm between the top of the ROV frame and the ice, to simulate field conditions, maximum output from thrusters at *in situ* pressure and water temperature. Distance between vertical thrusters and ice bottom was 55 cm. Based on the simulated flow velocities we calculated the shear stress (N m^{-2}) applied by the thrusters on the bottom of the ice, for an assumed logarithmic velocity distribution, and a bottom ice roughness of z_0 = 0.5 mm based on observations of under-ice flow fields (Crawford et al. 1999). Next, we carried out a field test (test C) to evaluate whether and to what extent the wakes of the thrusters disturbed or affected the ice algae biomass at the bottom of the ice. We established two parallel transects spaced 0.5 m apart with the ROV parked consecutively at nine predetermined positions at one transect, leaving one transect undisturbed. After parking of the ROV at the bottom of the ice we carefully drilled a 9 cm hole to retrieve the ice core. Positions were determined by the image based positioning system and position accuracy was checked based on the criteria that the hole was visible to the upwards directed camera. The ice cores were sampled using a 9 cm Kovacs ice corer driven with a battery-powered electrical drill. The lower 3 cm of each ice core was cut off for chlorophyll *a* (Chl *a*) analyses using a stainless steel saw. The Chl *a* is the dominant light absorbing pigment in phytoplankton and ice algae, and is a commonly used proxy for algae biomass due to a general linear relation between Chl *a* and ice algae biomass (Falkowski and Kiefer,1985). Ice samples were placed individually in zip-lock bags in a cooling box, and transported back to the laboratory at Kangerlussuaq International Science Support (KISS), and thawed overnight at 4°C in the dark. An exact volume between 0.25 and 0.5 liters of melted ice was filtered through glass fiber filters (GF75 Advantec) (0.75 μm), and these were packed and frozen at minus 18°C for transport to Denmark for Chl *a* analyses - see (Lund-Hansen et al., 2013) for details. This test assumes that any differences in Chl *a* concentrations between the two transects were related to disturbance by the ROV as Chl *a* concentrations were quite even within a small (0.5 m) spatial scale. Water samples from below the ice were collected using a bilge pump for determination of Chl *a* concentrations and processed as above.

2.8. Irradiance application tests

Under-ice irradiance spectrums were obtained with the TriOS spectroradiometer at stations with synchronous measurements of incident surface PAR ($PAR_{Surface}$) using a LiCor LI-192 sensor (Lincoln, Nebraska, U.S., http://www.licor.com). Surface PAR data were recorded as the average of 10 readings with 1 reading per second using a LiCor LI-250A meter with ROV parked at stations. Spectral irradiance between 400 and 700 nm from the spectroradiometer was integrated to give under-ice PAR at each station (PAR_{ROV}), and PAR transmittance was calculated as ($PAR_{ROV}/PAR_{Surface}$). A comparison of spectral derived PAR and PAR measured with the LiCor sensor in air was carried out and differences were very small (2-5 µm m^{-2} s^{-1}) at surface PAR of 450-600 µm m^{-2} s^{-1}. Transmittance also comprises 25 cm of sea water immediately below the ice as the distance between sensor head and ice bottom by the 4 spacer poles on the ROV (Fig. 1a-c).

2.9. Spatial resolution test

We marked 11 positions with a tape ruler to nearest 1 cm along a transect with a gradient of snow depths measured with a ruler to nearest 0.5 cm. PAR transmittance was measured with the ROV parked below the ice followed by ice coring and sampling for Chl *a* at the same positions applying the sampling procedures described above. Ice thickness was measured to the nearest 1 cm using a ruler.

3. Results

3.1. Positioning and performance of the ROV

Air temperatures varied between -5 and -20 °C and water temperatures below the ice were -1.5 °C, and weather was mostly calm with clear skies during the days of work on the ice. The ROV was easy to deploy through the hole in the ice by two persons and was easy to maneuver below by one ROV pilot. The positioning system working range was designed for 30 m but all tests were carried out with a maximum distance between reference poles of 15 m due to an unexpected higher light attenuation in the water below the ice (Fig. 1c). The higher light attenuation was related to higher (0.8 ± 0.2 mg m^{-3}) Chl *a* concentrations in the water as compared to a concentration of 0.12 ± 0.06 mg m^{-3} typical of previous years (Lund-Hansen et al., 2017). However, test A showed that the 5 cm diameter drilled holes were clearly visible (upwards camera) within the rectangle in 7 of 9 trials. The holes were visible to the camera but outside the rectangle in the two failed cases. The difference between the optical based position and the actual position, termed test B, showed an average difference of 28 ± 5 cm (n = 8) (Fig. 3a). The difference was negative, *i.e.* the distance between LED pole and the given optical position was shorter than the distance between LED pole and actual position, for the first part of the transect, and conversely positive for second part (Fig. 3a). The change from negative to positive deviation halfway, was probably related to the fact that the system only uses the distance measurements to the closest reference pole – D2 (Fig. 2c). The average offset from the transect line was 16 cm ± 5 cm (n = 8).

3.2. ROV and ice algae biomass

In test C regarding a possible disturbance of the algae we found a statistical significant ($p < 0.001$, $n = 9$) lower average Chl *a* concentration (1.92 ± 0.13 mg m^{-2}) after the ROV had been parked at positions, compared to the undisturbed transect (2.49 ± 0.14 mg m^{-2}). The average Chl *a* difference of 0.57 mg m^{-2} was quite consistent at all stations and equaled a loss of 23 percent (Fig. 3b). Based on the CFD simulations we calculated that the thrusters applied a shear stress of 0.1 N m^{-2} on the bottom of the ice at maximum output. A shear stress of 0.1 N m^{-2} is fairly high and can bring fine grained sediments in to suspension (Lund-Hansen et al., 2004). This is also, to our knowledge, the first estimate of a current shear stress that can flush away the ice algae, yet the critical shear stress is unknown, but clearly lower than 0.1 N m^{-2}.

3.3. Application for under-ice irradiance

We obtained 4 spectra below ice (79-80 cm thick) along a transect at nearly constant incident surface PAR (552.3 ± 8.0 µm photons m^{-2} s^{-1}) within 20 minutes with 3 snow depths (1.0, 5.5, and 11.0) and no snow. A comparison of irradiance spectra (400-700 nm) below the ice with no snow and three different snow depths showed a significant decrease in under-ice irradiance with increase in snow depths (Fig. 4a). The irradiance reduction was strongest in the red part of the spectrum (> 610 nm) leaving nearly no light below the ice with a 11 cm snow cover. We also found a strong ($r^2 = 0.97$, $n = 34$), and significant ($p < 0.001$) negative correlation between snow depth and PAR transmittance (T_{PAR}), transformed through $-\ln(T_{PAR})$ (Fig. 4b). Transmittance varied between a minimum of 0.1 and a maximum of 7.8%. The irradiance at 490 nm was least attenuated by the snow cover and the normalized differences index (NDI) analyses was applied to derive an index for snow depths, equivalent to the study by Mundy et al., (2007). Present NDI is of the form: NDI = [E(λ) – E(490)]/[E(λ) + E(490)], where λ is every other wavelength between 320-920 nm, and we scanned the irradiance–snow cover thickness dataset (n = 24) for the wavelength (λ) that gave the highest coefficient of determination (r^2) between NDI [E(490):E(λ)] and snow depth. The highest coefficient was found for NDI [E(490):E(610)] with a high ($r^2 = 0.76$) and significant ($p < 0.001$) negative correlation between NDI and snow depths (Fig. 4c). Experiments were carried out below a dry snow cover that was probably related to a period of strong winds about one week before we arrived at the site.

3.4. Spatial analyses

For spatial analyses we used the ROV at positions along a separate transect with a gradient of snow depths. Results substantiate the inverse relation between snow depths and PAR transmittance, and demonstrate a positive relation between PAR transmittance and algae biomass (Chl *a*) (Fig. 4d). With a spectroradiometer footprint radius of 0.5 m the sensor will receive 80% of the irradiance flux with a distance of 0.25 m between sensor head and bottom of the ice applying the eq. 1 in Nicolaus et al., (2010). With distances between positions of 0.93m–2.29m, there were little or no overlap of the effective footprints. The snow depth > 1.0 cm thick secured a diffuse light field below the ice (Petrich et al. 2012). The applied distance of 25 cm between sensor head and ice bottom provided a good spatial resolution of biomass and transmittance (Fig. 4d).

4. Discussion

4.1. The ROV

Deployment of ROVs below the ice in a polar environment with low temperatures and potential freezing of movable parts such as thrusters is a design challenge (Christ and Wernli, 2013). We considered this with pre-tests by placing the ROV in a freezer at - 30 °C to test thruster functionality at low temperatures, and a pressure test to 10 m depth in a saltwater basin below freezing point (– 1.6 °C). The working range of the ROV with the present configuration was 15 m and smaller to other ROVs used in Arctic and Antarctic under-ice work (Robison et al., 2011; Christ and Wernli, 2013; Katlein et al., 2015b). Tether length and the optical positioning system (*i.e.* the light attenuation in the water) both limited the working range. This was exemplified by our positioning tests that were carried out at a 15 m working range due to higher Chl *a* concentrations and increased light attenuation below ice than previously in Kangerlussuaq. However, this range was sufficient for the present aim of resolving variation in under-ice irradiances under landfast ice at a small horizontal scale. In the present study we did not experience any significant malfunction of the ROV or of any of its components other than a few minor failures such as replacement of a broken thruster and an Ethernet connector. However, that the wake of the thrusters was able to reduce ice algae biomass makes it necessary to redesign the way the ROV is taking off from under the ice. Now, the ROV fulfilled our immediate goals to design and deploy a low-cost ROV for accurate measurements of under-ice irradiance variability, and develop an ROV that is easy to deploy, maneuver below the landfast ice, and relocate. Using a X-box controller in combination with the thruster configuration provided an intuitive way of controlling the ROV that required little or no prior training. Experience was only needed when the ROV had to make small sideways displacements, where the tether could slightly pull on the ROV making it drift away from the desired position.

4.2. Positioning

Positioning is crucial when deploying ROVs and most solutions are acoustically based with sonar transducers placed below the water or ice surface, and with a transponder mounted on the ROV, as with the SCINI ROV, also designed for under-ice deployments (Cazenave et al., 2011). We have developed a new optically based positioning system, which was less expensive than any acoustic based solutions at the time of ROV design in October-November 2015. An acoustic solution would further obstruct the concept of designing a low-cost ROV. We were further concerned that acoustic signals could be distorted when operating at close ranges to the bottom of the ice. There are at present (February 2018) commercially available acoustic positioning systems for the price of about 5.000 USD (http://www.bluerobotics.com), though the precision of the system is yet unknown. Our measurements showed an average difference between optically based position and actual position of 28 ± 5 cm with an average offset, *i.e.* the perpendicular distance between transect line and center of ROV, of 16 ± 8 cm. The SCINI ROV for under-ice benthic research using sonar transducers had a similar precision of positioning with an average error of 27 cm between actual position and position of the ROV (Cazenave et al., 2011). The limitation of our optically based positioning could be caused by several issues, but based on the present study we identify three main factors. First factor is the calibration of the correlation between pixel count and angle, and distance. This calibration sequence conducted in fresh water basins could be improved giving a considerably better accuracy. The second factor is the physical placement of the cameras, where a slightly distorted camera would lead to a systematic error in angle computation. The third factor is how the data is being computed into the geometric properties (distance along and offset from line), where the current optical system only uses the required numbers to triangulate, thus disregarding the distance measurement to the reference pole the furthest away. Information from that pole could be used in the position calculations applying surveying techniques where more than one triangulation is applied to achieve a better accuracy and an estimation of error.

4.3. Applications

The deployments of the ROV enabled the positioning of the mounted spectroradiometer under the sea ice and facilitated non-invasive measurements of spectral irradiance and transmittance in this otherwise inaccessible environment. The measurements were used to quantify the relationship between snow depths and spectral attenuation of specific wavelengths as for the present NDI (490:610). Chl *a in vivo* has absorption peaks around 440 nm and 667 nm (Bricaud et al., 2004) and no large absorption peaks centered around 490 and 610 nm. The index is then only insignificantly influenced by the presence of the algae, and especially at the low ice algae concentrations found in Kangerlussuaq around 1-2 mg Chl a m^{-2}. Mundy et al. (2007) found little effect on spectral composition below the ice between 400 and 550 nm related to a snow cover, which corroborates with our results of minimum attenuation at 490 nm with a snow cover. Nicolaus et al. (2013) also found minimum attenuation around 500 nm. In the present study ice algae biomass was reduced by the wakes of the thrusters and deriving a biomass NDI was not pursued any further. The importance of a snow cover in determining ice algae biomass and photosynthesis on the underside of sea ice has been clearly demonstrated in several studies (Mundy et al., 2005;

Juhl and Krembs, 2010; Lund-Hansen et al., 2013). This strongly emphasizes the need for a good description of transmittance and under-ice spectral composition as ice algae only absorbs light at specific wavelengths, as mentioned above. For instance, present data showed that the spectral composition of the under-ice irradiance depends on snow depths where there was virtually no red light (> 610 nm) below the ice at 11 cm snow depth, which is ecologically significant as ice algae exhibit a strong absorption peak at 667 nm (Bricaud et al., 2004). Previous studies have shown a general negative relation between snow depths and PAR transmittance (Mundy et al., 2005; Juhl and Krembs, 2010), and here we obtained a high and statistically significant correlation between snow depths and -ln(T_{PAR}). Similar correlations between ice thickness of ponded and bare ice and T_{PAR} have been established but with lower correlation coefficients (Light et al., 2015). Transmittance is transformed with natural logarithm as transmittance decreases exponentially with pathway length (Kirk, 1994). Irradiance is scattered and absorbed in sea ice though less than in the snow (Perovich et al., 1990), but irradiance attenuation in the ice is here considered a constant as sea ice thickness only varied about 1 cm between 79 and 80 cm. We further assumed that optical constituents as particulate matter, brine and gas volumes that affect transmittance did not change within the limited time-scale and small horizontal distances applied here. There were algae present at the bottom of the ice but in so low concentrations (1-2 mg m^{-2}) that their absorption effects on PAR transmittance can be assumed to be minimal, which leaves only the snow to be the main factor for the variability in transmittance. The 25 cm of water column between spectroradiometer head and ice bottom contained phytoplankton, and PAR was reduced by 7.7% between bottom of the ice and sensor head, using a K_d(PAR) = 0.32 m^{-1} obtained below the ice in Kangerlussuaq previously (Lund-Hansen et al., 2018). Further, the phytoplankton is evenly distributed below the ice, and thus the small reduction is similar at all positions. Given that the snow is the main factor for the T_{PAR} variability, the strong correlation between snow depths and T_{PAR} demonstrates that the ROV works well and that the design is applicable for such optical under-ice studies. It is strongly supposed that applying a short, and here 25 cm, and constant distance between bottom of the ice and sensor head with parking of the ROV during measurements improved the results obtained. ROVs for measuring under-ice irradiance fields generally fly about 1-2 m below the ice (Nicolaus et al., 2012; Katlein et al., 2015b) whereas a shorter distance (5-10 cm) can be obtained with through hole L-arms (Lund-Hansen et al., 2013; Lange et al., 2016) but it is difficult to obtain same distance at all positions.

5. Conclusions

In view of the technical challenges of working in the Arctic at water and air temperatures well below zero with a low-cost ROV, we consider the tested ROV design and set-up for being suitable for measuring under-ice irradiance in level landfast sea ice. The optically based positioning system proved to be a good and reliable solution where positions we retrieved within specified uncertainties, which could be reduced even further by an improved calibration. With this ROV we obtained high correlations between snow depths and PAR transmittance, as well as a new NDI index for snow cover thickness applicable in future similar studies. The ROV can be improved to avoid or strongly reduce any disturbance of the ice algae located at the bottom of the ice.

Acknowledgements

The project received financial support from The Danish Council for Independent Research (Project DFF – 1323-00335, Sea ice ecosystems: Ecological effects of a thinning snow cover), The Carlsberg Foundation, Aarhus University, and the Brdr. Hartmann Foundation. Thanks to Basse Vængtoft, Rikka Møller, and Chi Kim Thi Pham at KISS for logistical assistance and help. Thanks to two anonymous reviewers who helped to improve the manuscript.

References

Arndt, S., Meiners, K.M., Ricker, R., Krumpen, T., Katlein, C., Nicolaus, M., 2017. Influence of snow depth and surface flooding on light transmission through Antarctic pack ice. J. Geophys. Res. 122, 2108-2119, http://doi.org/10.1002/2016JC012325

Arrigo, K.R., Sullivan, C.V., 1994. A high resolution bio-optical model of microalgal growth: test using sea-ice algal community time-series data. Limnol. Oceanogr. 39, 609-631, http://doi.org/10.4319/lo.1994.39.3.0609

Arrigo, K.R., Mock, T., Lizotte, M.P. 2010. Primary producers and sea ice. In: Thomas, D.N., Dieckmann, G.S. (eds.) Sea ice. Wiley-Blackwell, Chichester, p. 283−326, http://doi.org/10.1002/9781444317145.ch8

Ambrose, W. G., Quillfeldt, C.V., Clough, L.M., Tilney, P.V.R., Tucker, T. 2005. The sub-ice algal community in the Chukchi sea: large- and small-scale patterns of abundance based on images from remotely operated vehicle. Pol. Biol. 28, 784-795, http://doi.org/10.1007/s00300-005-0002-8

Bowen, A.D., Yoerger, D.R., German, C.C., Kinsey, J.C., Jakuba, M.V., Gomez-I., D., Taylor, C.L., Machado, C., Howland, J.C., Kaiser, C.L., Heintz, M., Pontbriand, C., Suman, S., O'Hara, L., Bailey, J., Judge, C., McDonald, G., Whitcomb, L.L., McFarland, C.J., Mayer, L., 2014. Design of *Nereid-UI*: A remotely operated underwater vehicle for oceanographic access under ice. Oceans – St. John's 33, 1-6 http://doi.org/10.1109/OCEANS.2014.7003125

Bricaud, A., Claustre, H., Ras, J., Oubelkheir, K., 2004. Natural variability of phytoplankton absorption in oceanic waters: Influence of the size structure of algal populations. J. Geophys. Res C11010, http://dx.doi.org/10.1029/2004/JC002419

Christ, R., Wernli, R., 2013. The ROV Manual. Butterworth Heinemann 2nd Edition, Oxford. 712 pp.

Cazenave, F., Zook, R., Carroll, D., Flagg, M., Kim, S. 2011. Development of the ROV SCINI and deployment in McMurdo Sound, Antarctica. J. Ocean. Techn. 3, 40-58, http://digital.mlml.calstate.edu/islandora/object/ir%3A922

Crawford, G., Padman, L., McPhee, M., 1999. Turbulent mixing in Barrow Strait. Cont. Shelf. Res. 19, 205-245, https://doi.org/10.1016/S0278-4343(98)00086-7

Falkowski, P., Kiefer, D.A., 1985. Chlorophyll *a* fluorescence in phytoplankton: relationship to photosynthesis and biomass. J. Plankton. Res. 7, 715-731, http://doi.org/10.1093/plankt/7.5.715

Hobson, B.W., Sherman, A.D., McGill, P.R., 2011. Imaging and sampling beneath free-drifting icebergs with a remotely operated vehicle. Deep-Sea Res. II, 58, 1311-1317, https://doi.org/10.1016/j.dsr2.2010.11.006

Juhl, A.R., Krembs, C., 2010. Effects of snow removal and algal photoacclimation on growth and export of ice algae. Pol. Biol. 33, 1057-1065, http://doi.org/ 10.1007/s00300-010-0784-1

Katlein, C., Fernández-Mendéz, M., Wenzhöfer, F., Nicolaus, M., 2015. Distribution of algal aggregates under summer sea ice in the Central Arctic. Pol. Biol. 38, 719-731, http://doi.org/10.1007/s00300-014-1634-3

Katlein, C., Arndt, S., Nicolaus, M., Perovich, D.K., Jakuba, M.V., Suman, S., Elliott, S., Whitcomb, L.L., McFarland, C.J., Gerdes, R., Boetius, A., German, C.R., 2015b. Influence of ice thickness and surface properties on light transmission through Arctic sea ice. J. Geophys. Res. 120, 5932-5944, http://doi.org/10.1002/2015JC010914

Katlein, C., Hoppmann, M., Nicolaus, M., Coppolaro, M., Belter, J., 2017. First results from a new interdisciplinary robotic vehicle for under-ice research. Arctic Frontiers 2017, Tromsö, Norway. http://doi.org.10013/epic.50316

Kirk, J.T.O., 1994. Light and Photosynthesis in the aquatic ecosystems. 2nd Edition, Cambridge University Press. 509 pp.

Lange, B.A., Katlein, K., Nicolaus, M., Peeken, I., Flores, H., 2016. Sea ice chlorophyll a concentrations derived from under-ice spectral radiation profiling platforms. J. Geophys. Res. 121, 8511-8534, http://doi.org /10.1002/2016JC011991

Light, B., Perovich, D.K., Webster, M., Polashenski, C., Dadic, R., 2015. Optical properties of meelting first-year Arctic ice. J. Geophys. Res., JCO11163, http://doi.org/10.1002/2015JC011163

Lund-Hansen, L.C., Pejrup, M., Floderus, S., 2004. Pelagic and seabed fluxes of particulate matter and carbon, and C:N rations resolved by sediment traps during a single bloom, southwest Kattegat. J. Sea Res 52, 87-98, https://doi.org/10.1016/j.seares.2003.11.003

Lund-Hansen, L.C., Hawes, I., Nielsen, M.H., Dahllöf, I., Sorrell, B.K., 2018. Summer meltwater an spring sea ice primary production, light climate and nutrients in an arctic estuary, Kangerlussuaq, West Greenland. Arctic, Alpine and Antarctic Research 50, https://doi.org/10.1080/15230430.2017.1414468

Lund-Hansen, L.C., Hawes, I., Sorrell, B.K., Nielsen, M.H., 2013. Removal of snow cover inhibits spring growth of Arctic algae through physiological and behavioral effects. Pol. Biol. 37, 471-481, http://doi.org/10.1007/s00300-013-1444-z

Meiners, K.M., Arndt, S., Bestley, S., Krumpen, T., Ricker, R., Milnes, Newbery, K., Freier, U., Jarman, S., King, R., Proud, R., Kawaguchi, S., Meyer, B., 2017. Antarctic pack ice algal distribution: Floe-scale spatial variability and predictability from physical parameters. Geophys. Res. Lett. 44, 7382-7390, http://doi.org/10.1002/2017GL074346

Moore, D.J., Jolly, J., Geisel, F., 1986. A small lightweight ROV for studies under Arctic ice. *In* Wernli, R.L., and R. Chapman (eds.), ROV '86: Remotely Operated Vehicles, Springer Verlag, Berlin, pp 360-366, http://doi.org/10.1007/978-94-009-4207-3_30

Mundy, C.J., Barber, D.G., Michel, L., 2005. Variability of snow and ice thermal, physical and optical properties pertinent to sea ice algae biomass during spring. J. Mar. Res. 58, 107-120, http://doi.org/10.1016/j.jmarsys.2005.07.003

Mundy, C.J., Ehn, J.K., Barber, D.G., Michel, C., 2007. Influence of snow cover and algaee on the spectral dependence of transmitted irradiance through Arctic landfast first-year ice. J. Geophys. Res. 112, C03007, http://doi.org/10.1029/2006JC003683

Nicolaus, M., Hudson, S.R., Gerland, S., Munderloh, K., 2010. A modern concept for autonomous and continuous measurements of spectral albedo and transmittance of sea ice. Cold Reg. Sci. Tech. 62, 14-28, http://doi.org/10.1016/j.coldregions.2010.03.001

Nicolaus, M., Katlein, C., Maslanik, J., Hendricks, S., 2012. Changes in Arctic sea ice result in increasing light transmittance and absorption. Geophys. Res. Lett. 39, L24501, http://doi.org/10.1029/2012GL053738

Nicolaus, M., Katlein, C., 2013. Mapping radiation transfer through sea ice using a remotely operated vehicle (ROV). T. Cryosph. 7, 763-777, http://doi.org/10.5194/tc-7-763-2013

Nicolaus, M., Petrich, C., Hudson, R., Granskog, M.A., 2013. Variability of light transmission through Arctic land-fast ice during spring. Chryosphere 7, 977-986, http://doi.org/10.5194/tc-7-977-2013

Nielsen, M.H., Erbs-Hansen, D.R., Knudsen, K.L., 2010. Water masses in Kangerlussuaq, a large fjord in west Greenland: the processes of formation and the associated foraminiferal fauna. Pol. Res. 29, 159-175, http://doi.org/10.1111/j.1751-8369.2010.00147.x

Perovich, D.K. 1990. Theoretical estimates of light reflection and transmission by spatially complex and temporally varying sea ice covers. J. Geophys. Res. 95, 9557– 9567, http://doi.org/10.1029/JC095iC06p09557

Perovich, D.K., Roesler, C.S., Pegau, W.S., 1998. Variability in Arctic sea ice optical properties. J. Geophys. Res. 193, 1193-1208, http://doi.org/10.1029/97JC01614

Petrich, D.K., Nicolaus, M., Gradinger, R., 2012. Sensitivity of the light field under sea ice to spatially inhomogeneous optical properties and incident light assessed with three-dimensional Monto Carlo radiative transfer simulations. Cold Reg. Sci. Tech. 73, 1-11, https://doi.org/10.1016/j.coldregions.2011.12.004

Robison, B.H., Vernet, M., Smith, K.L., 2011.Algal communities attached to free-drifting Antarctic icebergs. Deep-Sea Res. II, http://doi.org/10.1016/j.dsr2.2010.11.024

Taskjelle, T., Hudson, S.R., Granskog, M.A., Nicolaus, M., Lei, R., Gerland S., Stamnes, J.J., Hamre, B., 2016. Spectral albedo and transmittance of thin young Arctic sea ice. J. Geophys. Res.121, http://doi.org/10.1002/2015JC011254

Wadhams, P. 2012. Arctic Ice Cover, Ice Thickness and Tipping Points. AMBIO, 41, 23-33, http://doi.org/10.1007/s13280-011-0222-9

Figure legends

Fig. 1. a) The ROV with payload ready for deployment through hole a (75×50 cm) in the ice, b) a reference pole with LEDs for image based positioning, c) the ROV parked below the ice with the LED reference pole in the distance and drilled holes 9 cm for Chl *a* sampling, d) ROV set-up on the ice at deployments with control room. Reference poles with LEDs below the ice form a straight line path with a fixed distance between the LEDs, e) the ROV is deployed through a hole in the ice.

Fig. 2. a) The reference poles with LEDs (see also Fig. 1d) are filmed and the horizontal pixel count (px_h) to the middle of the image, and the vertical pixel count (px_v) between the two lights are both continuously measured with the ROV mounted camera, b) the vertical pixel count px_v is used to determine the distance to each of the reference poles, and horizontal pixel count px_h is used to correct for sideward drift and orientation as to keep $px_h = 0$. The smaller the distance between reference pole and ROV, the higher the px_v The relationship results in a regression formula between the distance to the reference pole and px_v, depending on the fixed parameters, *i.e.* the camera chip size (CCD sensor), field of view of the lens, the medium (water), depth and the distance between the LEDs, c) a cartoon of the ROV between the two LED poles, with angles α_f (front) and α_r (rear) between center axis of ROV and direction to poles. Positions were determined using α_f (front) and α_r (rear) at all times and the distance to the nearest pole D2.

Fig. 3. a) Chl *a* concentrations (mg m^{-2}) at positions along a transect without (no ROV at any of the positions) and a transect with ROV parked below the ice at positions for optical measurements, b) grey bars are deviation (cm) between calculated ROV position and actual position along the transect and black bars are the perpendicular deviation (cm) (offset) from transect line.

Fig. 4. a) Under-ice irradiance (mW m^{-2} nm^{-1}) in the PAR band (400-700 nm) at three snow depths (1.0, 5.5, and 11.0 cm) and with no snow, and note that 5.5 and 11.0 cm of snow depths refer to secondary y-axis for scaling purposes, b) the relation between snow depths (cm) and PAR transmittance (T_{PAR}) as -ln(T_{PAR}) and T_{PAR} (%) on secondary y-axis, c) relation between snow depth (cm) and the snow NDI, d) PAR transmittance (T_{PAR} (%), Chl *a* (mg m^{-2}), and snow depths (cm) along a transect. Note that Chl *a* has been multiplied by 6 for scaling purposes. Ice thickness was 79-80 cm at positions.

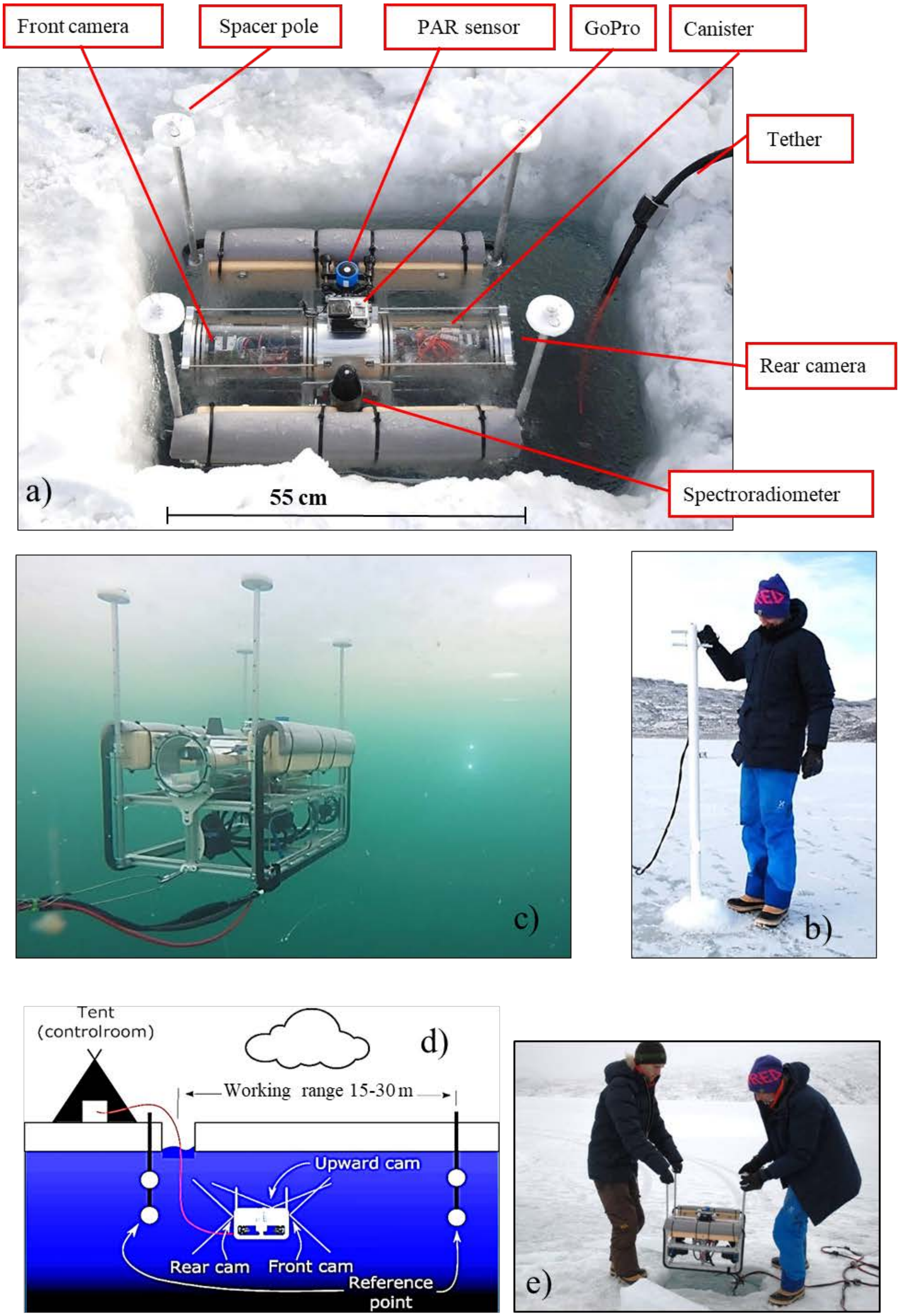

Front camera
Spacer pole
PAR sensor
GoPro
Canister
Tether
Rear camera
Spectroradiometer
a)
55 cm
c)
b)
Tent
(controlroom)
d)
Working range 15-30 m
Upward cam
Rear cam
Front cam
Reference
point
e)

Fig. 1

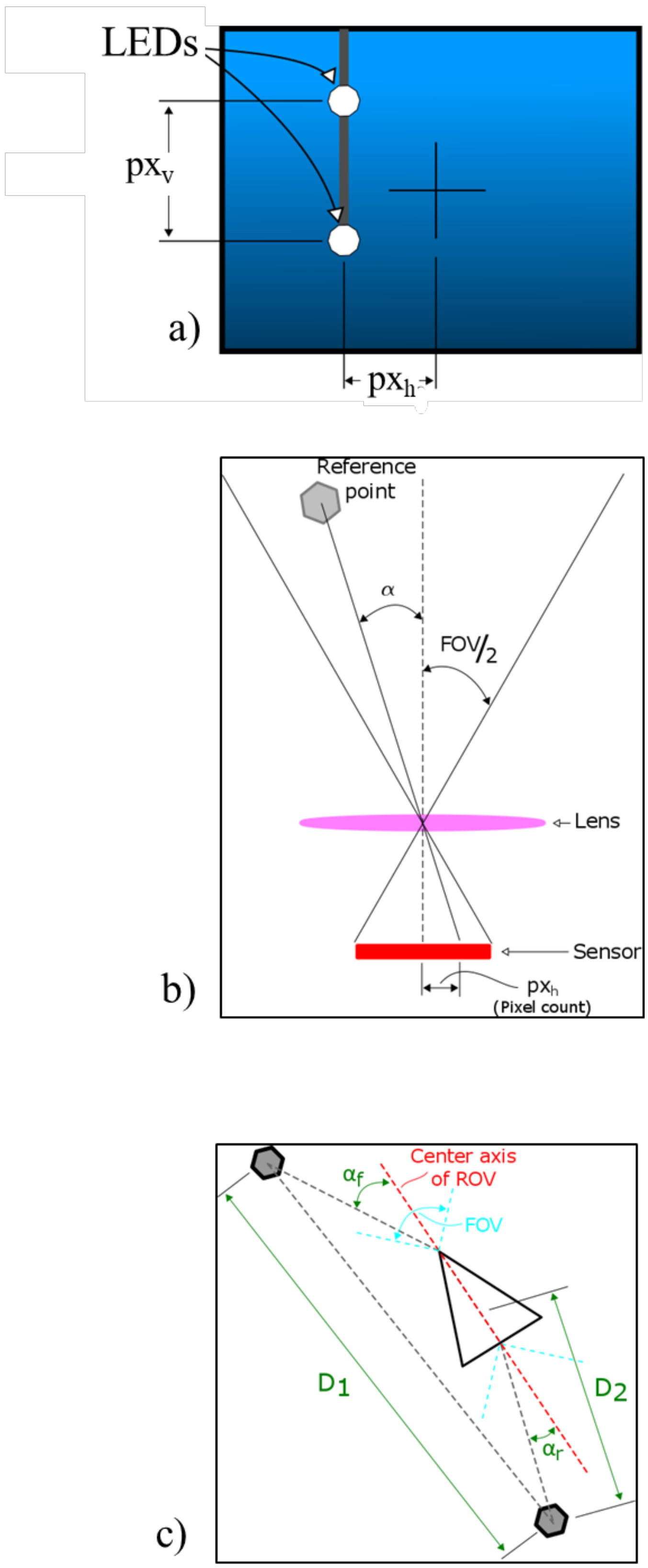
LEDs
px_v
a)
px_h
Reference point
α
FOV/2
Lens
Sensor
px_h
(Pixel count)
b)
Center axis of ROV
α_f
FOV
D_1
D_2
α_r
c)

Fig. 2

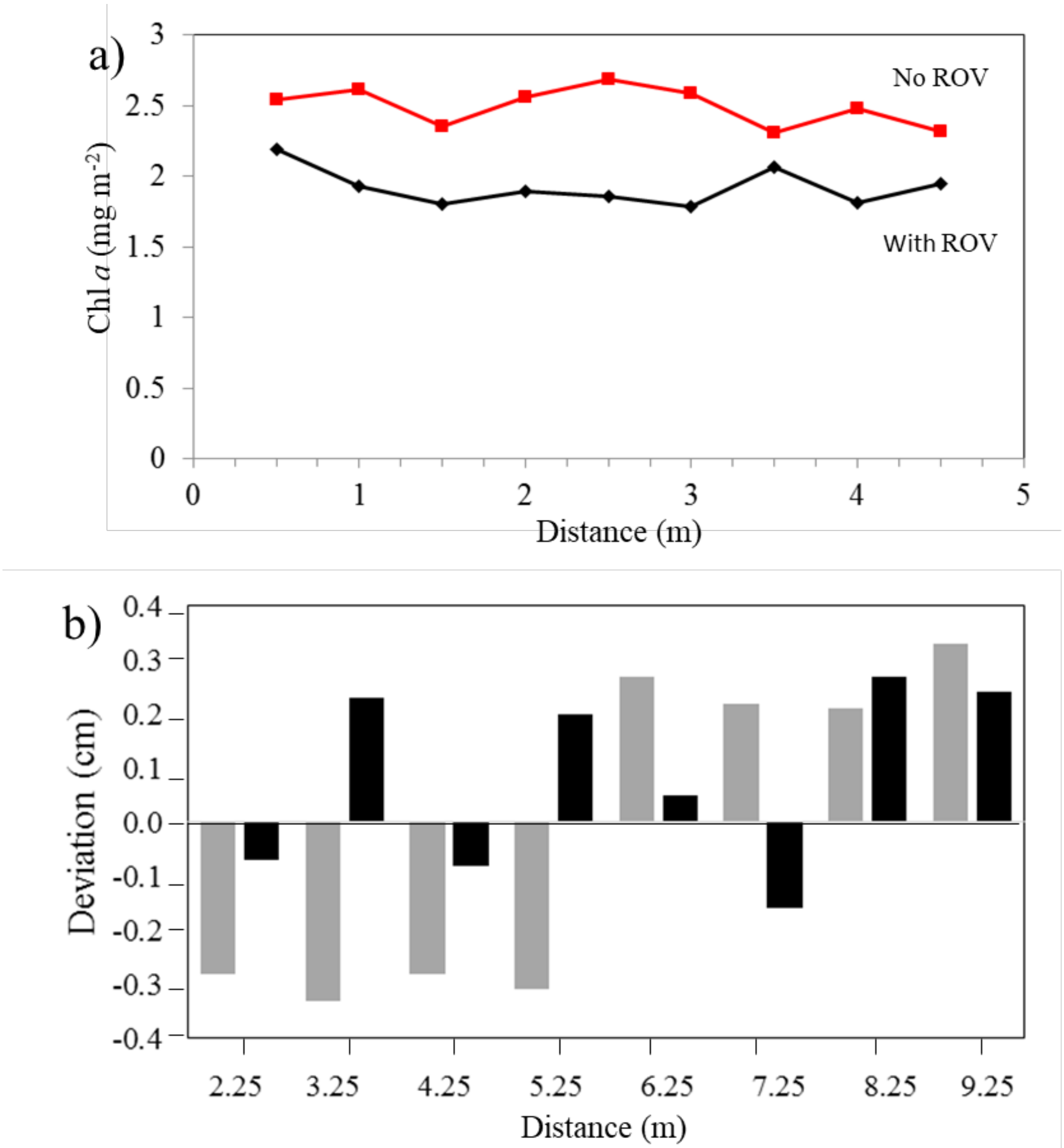
a)
Chl a (mg m-2)
No ROV
With ROV
Distance (m)
b)
Deviation (cm)
2.25
3.25
4.25
5.25
6.25
7.25
8.25
9.25
Distance (m)

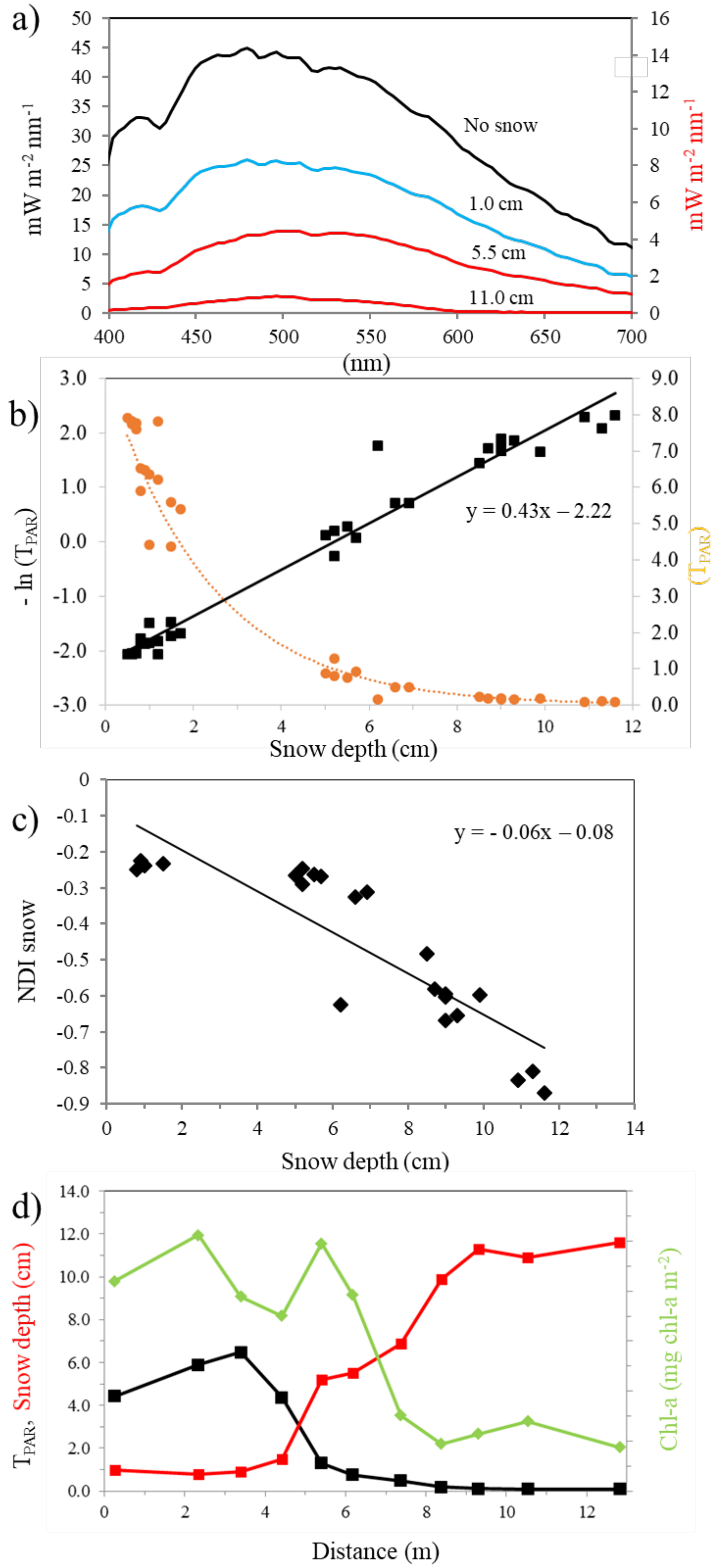
a)
mW m-2 nm-1
mW m-2 nm-1
No snow
1.0 cm
5.5 cm
11.0 cm
(nm)
b)
- ln (TPAR)
(TPAR)
y = 0.43x – 2.22
Snow depth (cm)
c)
NDI snow
y = - 0.06x – 0.08
Snow depth (cm)
d)
TPAR, Snow depth (cm)
Chl-a (mg chl-a m-2)
Distance (m)